NASA Technical Memorandum 78963

THERMAL-STRUCTURAL MISSION ANALYSES OF AIR-COOLED GAS TURBINE BLADES

Albert Kaufman and Raymond E. Gaugler
Lewis Research Center
Cleveland, Ohio

TECHNICAL PAPER to be presented at the
International Gas Turbine Conference
sponsored by the American Society of Mechanical Engineers
San Diego, California, March 11-15, 1979

THERMAL-STRUCTURAL MISSION ANALYSES OF AIR-COOLED GAS TURBINE BLADES

ALBERT KAUFMAN and RAYMOND E. GAUGLER
NASA-Lewis Research Center
Cleveland, Ohio 44135

ABSTRACT

Cyclic temperature and stress-strain states in cooled turbine blades were calculated for a simulated mission of an advanced technology aircraft engine. TACT1 (three dimensional heat transfer) and MARC (nonlinear structural analysis) computer programs were used to analyze impingement cooled airfoils, with and without leading-edge film cooling. Creep was the predominant damage mode, particularly around film cooling holes. Radially angled holes exhibited less creep than holes normal to surface. Beam-type analyses of all-impingement cooled airfoils gave fair agreement with MARC results for initial creep.

INTRODUCTION

Cooled airfoils in high-pressure turbine stages of advanced aircraft engines are subject to creep during steady-state operation and plastic flow during the thermal transients. In order to calculate the airfoil cyclic lives, it is necessary to determine the transient and steady state temperatures and the accumulated inelastic strains over the entire engine mission.

In recent years, nonlinear finite element programs such as MARC (1,2) have become available for the three dimensional analysis of structures involving cyclic creep and plasticity. Aside from a limited use as analytical research tools, these nonlinear programs have not been utilized in turbine blade design because of the extensive work and computing times involved. Quantitative accuracy with nonlinear, finite element programs is at present precluded because of the lack of cyclic turbine material properties, particularly cyclic creep properties, and by the necessity to limit the analyses to a few cycles due to the computing times required.

The primary purpose of this study was to gain a greater understanding of blade damage modes, film cooling hole effects and effects of small changes in gas profile on cooled blades in advanced engines through the use of a nonlinear three dimensional structural analysis program. A secondary purpose was to evaluate the applicability of a simpler one dimensional beam-type program representative of most current blade cyclic analysis practice.

The airfoil temperatures and stress-strain states in the three impingement cooled rotor blades (two with leading-edge film cooling holes) were studied using an advanced transient thermal analysis program, TACT1 (3), and the MARC nonlinear structural analysis program. The thermal-structural analyses were based on a mission which simulated the takeoff, climb, cruise and descent conditions of an advanced technology aircraft engine. Airfoil temperatures, stresses, strains and predicted creep lives are compared for four cases: the two leading-edge film cooled blades with a typical gas temperature profile and the blade without cooling holes with both typical and slightly flatter gas temperature profiles.

ANALYTICAL PROCEDURE

Conditions of Analyses

The analyses were based on the operating conditions of a first stage turbine blade in an advanced high-bypass ratio turbofan engine being studied for use in the 1990 time period. The blade airfoil is 3.8 cm in both span and chord and has a hub-to-tip radius ratio of 0.85. The primary blade cooling system analyzed was an all-impingement cooled con-

figuration which used an internal insert from which coolant air flowed through an array of holes to impinge on the inner surface of the blade shell. In two cases, a single row of film cooling holes at the leading edge was also considered. The assumed blade material was cast IN 100 alloy. Stress-strain and creep rupture properties for this alloy were obtained from (4).

The assumed flight mission for this engine consisted of a 5 second transient from idle to maximum takeoff, a 5 minute hold at maximum takeoff, a 30 minute hold at maximum climb, a 90 minute hold at cruise and a 5 second transient from cruise back to idle. The mission cycle was divided into 34 time increments for the analysis. Two gas temperature profiles were considered in this study: a typical and a somewhat flatter profile. For the profile which represented typical gas conditions, the blade relative effective gas temperature at midspan cycled between 679° C at idle and 1400° C at maximum takeoff. The flatter gas profile cycled between midspan temperatures of 669° C at idle and 1378° C at maximum takeoff. At maximum takeoff, the gas inlet total pressure was 2858 kPa. The coolant-to-gas flow ratio at each operating point was held essentially constant for all the cooling configurations under study (0.116 to 0.118 at maximum takeoff).

Four analytical cases were studied (table I); an all-impingement cooled airfoil using both the typical (A) and flatter (B) gas profiles and two impingement cooled airfoils with film cooled leading edges using gas profile A. The configurations with film cooled leading edges had a single row of 0.05 cm diameter holes spaced 10 diameters apart; one configuration had the holes normal to the surface and the other had the holes angled 30° to the surface in the spanwise direction.

Analytical Methods

Transient and steady-state temperatures were computed with the TACT1 thermal analysis program. TACT1 was developed at the NASA Lewis Research Center to compute time-dependent three dimensional temperature distributions in airfoils cooled by impingement and crossflow convections. Coolant side heat transfer coefficients were calculated in the program using published correlations. The program also has the capability to handle limited film cooling, using a correlation for effectiveness based on reducing the film cooling holes to an equivalent slot. Temperature gradients around the hole and the effect of hole angle were not considered. The calculated metal temperatures are estimated to be accurate within about 70° C, based on the experimentally determined accuracy of the correlations used to calculate heat transfer coefficients.

Airfoil stress-strain states as a function of mission time were computed using the MARC nonlinear, finite-element structural analysis program. This program has the capability of performing cyclic plastic and creep strain calculations in a series of time increments for a series of engine missions. In the analyses presented in this paper, the computations were continued until the start of descent on the second mission cycle in order to eliminate from consideration the nonrecurring plastic strain induced during the initial mission. Although MARC has an integrated thermal analyzer option, it requires specification of the coolant temperature and heat transfer coefficient at each nodal point. Since the TACT1 program would have to be run to get this information, it was decided to bypass the MARC thermal analyzer and use the output metal temperatures from TACT1 directly.

Plastic strain behavior was based on the incremental theory of plasticity using the von Mises yield criterion. Although a number of hardening rules were considered, including kinematic hardening, there was never sufficient stress reversal during the descent part of the mission to cause reversed plastic flow. It is possible that some plastic strain reversal would have been calculated if the mission cycle had included the thrust reversal or cool down portions of the flight or local temperature gradients around the holes had been taken into account. Material creep behavior was represented by a von Mises yield criterion and the creep rate, $\dot{\epsilon}_c$, by an exponential creep law of the form $\dot{\epsilon}_c = A\sigma^n$ where A and n are dependent on temperature and independent of the stress, σ. Centrifugal and gas pressure loads and local metal temperatures from TACT1 for each mission increment were input and calculated stresses and strains output at each of 27 Gaussian integration points in each element. The centrifugal loading included the mass of the impingement insert and a tip cap. Although temperature-stress-strain results are presented for the inner and outer surfaces of the airfoil shell in this paper, these results actually come from calculational stations inside the wall at a distance from the surface of about 11 percent of the local wall thickness.

Structural analyses were also performed using a one dimensional, beam-type program (5). The one dimensional analyses were based on the same thermal and mechanical loading cycles and material properties as were used in the MARC analyses and included the effects of centrifugal restoring moments.

Finite Element Analysis

The finite element model of a leading-edge film cooled airfoil configuration (case 3) is illustrated in Fig. 1. The airfoil configurations were modelled with 20 node, isoparametric, three dimensional elements. The finite element network for the leading-edge film cooled airfoil had 46 elements with 405 nodes and the all-impingement cooled airfoil had 39 elements with 349 nodes. Nodes at the hub of the airfoil model were fixed in the radial direction. Because of the great amount of computer time required for the analyses, a finer mesh than that shown in Fig. 1 was not feasible. Each mission cycle required from 15 to 20 hours of accumulated Univac 1110 computer time. Although these computer times could be reduced substantially with some of the faster machines available, the use of nonlinear, three dimensional structural programs as practical design tools is probably dependent on further advances in computer technology.

Because of limitations of computer storage and speed, only one leading edge hole was modelled. A check of the accuracy of the analysis for the film-cooled model of Fig. 1 with the hole axis normal to the surface (case 3) was obtained by subjecting the airfoil to a uniformly distributed mechanical stress in the spanwise direction at a uniform temperature. An elastic stress concentration factor of 2.85 was obtained for a calculational station 0.003 cm from the hole rim; this compares to a theoretical stress concentration factor of 3.0 at the rim of a central hole in a plate subjected to a uniaxial mechanical load.

An error is introduced into the analysis by only modelling one hole since the presence of adjacent holes tends to reduce the stress concentration factor and the local wall stiffness. In Peterson (6), the

theoretical stress concentration factor for a plate with a single row of holes and a tensile load in the direction of the line of the holes is shown to be 2.9 for a spacing of 10 diameters compared to 3.0 for a single hole. In order to give consideration to these effects, the film cooling hole in the finite element model was placed at one sixth of the span height from the airfoil hub rather than at one-third span which would be a slightly more critical span location. The one-sixth span position was also a somewhat more convenient location for modelling a radially angled hole.

RESULTS AND DISCUSSION

Cyclic Metal Temperatures

Computed airfoil leading edge stagnation point, trailing edge and average (defined as weighted temperatures of the cross section) temperatures at midspan are shown in Fig. 2 as a function of elapsed time during the mission for cases 1 and 3. The thermal cycles for cases 3 and 4 are identical because of the assumptions used in the heat transfer procedure.

A number of features are common to the midspan metal temperature transients for all four cases. Throughout the mission the leading-edge inside wall temperature was colder than the average temperature; therefore, the thermal stresses were always tensile and additive to the centrifugal stresses. The outside wall temperatures at the leading and trailing edges were always hotter than the average temperature during takeoff, climb and cruise indicating compressive thermal stresses at these locations. At maximum takeoff condition, where the gas pressure was highest, the temperature difference between the leading edge inside and outside surfaces was about 150° C at midspan. The maximum metal temperature reached during the mission was about 1050° C for all four cases and occurred at maximum takeoff.

The thermal response for case 2 was similar to that shown for case 1 in Fig. 2(a) except for a reduction in the leading edge, trailing edge and average midspan temperatures of about 11° C at the takeoff, climb and cruise hold time conditions; the overall bulk temperature did not change when comparing cases 1 and 2. Compared to all-impingement cooling (Fig. 2(a)), film cooling (Fig. 2(b)) resulted in a leading edge outside surface temperature about equal to the average temperature at climb, and colder than the average temperature throughout the descent. The average midspan and bulk temperatures of the film cooled airfoil, although lower at maximum takeoff and climb, were about the same at cruise compared to the all-impingement cooled airfoil (Fig. 2(a)). Typical metal temperature contours at cruise for the outside surfaces of the airfoil pressure and suction sides are presented in Fig. 3 for case 1, which was used as the baseline case.

Effective Stress-Strain Distributions

Typical effective stress and inelastic strain contours for the end of cruise on the second cycle are shown in Fig. 4 for case 1 at the surfaces where the maximum values occurred. As expected, the maximum stresses were at the inside walls where temperatures were coldest and at the airfoil hub in the all-impingement cooled configurations (Fig. 4(a)) where centrifugal stresses were highest and at the hole rim in the film cooled configurations.

Results of the analyses indicated, as will be discussed later, that the predominant damage mode for all four cases was creep. The location of maximum creep strain (henceforth called the "critical location") was at the inside wall of the leading edge region at the 33 percent span height for cases 1 (Fig. 4(b)) and 2 and adjacent to the hole rim for cases 3 and 4. The critical locations for the all-impingement cooled configurations were slightly to the suction side of the leading edge in case 1 and slightly to the pressure side of the leading edge in case 2. The effective total strains at the critical location were either the highest or close to the highest total strain values in the airfoils. Case 4 was unusual in that the critical location shifted from the suction side of the film cooling hole on the first cycle to the pressure side of the hole on the second cycle.

The plastic strains for all cases were only incurred during the takeoff transient on the initial mission. The highest plastic strains occurred at the leading edge at 33 percent span on the outside surface for the all-impingement cooled blades (Fig. 4(a)) and on the inside surface at the hole rim for the film cooled blades.

Effective Strain Cycles

Effective total strain-temperature cycles for the critical airfoil locations are presented in Fig. 5 for the period between the end of cruise for the first and second missions. The highest total strains were reached during maximum takeoff. The total strain levels, ranges and ratcheting were considerably greater for the film cooled cases 3 and 4 than for the all-impingement cooled cases 1 and 2. Even though the total strain levels change under repeated cycling due to the creation of residual strains, the total strain range tends to be constant.

Accumulated effective creep strains at the critical locations are shown in Fig. 6 up to the end of cruise of the second mission cycle where the analysis terminated. The largest creep strain changes took place during cruise for cases 1, 2, and 4 and during the maximum takeoff hold time for case 3. Progressive stress relaxation under cycling caused a 35 to 45 percent reduction in the creep strain increment for cases 1 to 3 and a 72 percent reduction for case 4 during the second mission cycle as compared to the first cycle. Although case 4 shows the highest creep strain level in Fig. 6, the creep increment for the second cycle was less than case 3 because of the greater creep relaxation.

The strain cycles shown in Figs. 5 and 6 are summarized in Table II. Also presented are the maximum effective total strains reached on the first cycle; these values should be approximately equivalent to the total strain ranges for a cycle where the engine is shut down at the completion of every mission.

Using case 1 as a basis of comparison, the major effect of the flatter gas temperature profile was to decrease the creep strain range per cycle about 20 percent. There was also an increase in total strain range for case 2, but the total strain levels for both all-impingement cooled cases are too small to have any significant effect on blade life. Leading edge film cooling holes in case 3 increased the creep strain range by 100 percent and the total strain range by 230 percent for the candidate mission and 150 percent for an engine shutdown after each mission. Angling the holes 30° radially to the surface (case 4) resulted in smaller total strain and creep strain increments per cycle than having the holes normal to the surface (case 3). The increases in strain ranges in case 4 compared to case 1 were 39 percent in creep

strain, 220 percent in total strain for the mission, and 120 percent for an engine shut down after each mission.

Comparison of 1D and 3D Analyses

One dimensional beam-type analyses were also performed for cases 1 and 2 for the 33 percent airfoil span section. The maximum total and creep strain changes per cycle from the two analytical methods are compared in Table II.

The critical airfoil location from the one dimensional analysis was to the suction side of the leading edge region (location B in Fig. 7), whereas the critical locations from the MARC analyses were somewhat closer to the leading edge (location A for case 1 and location C for case 2 in Fig. 7). Using the one dimensional analysis, computed creep strain increments per cycle up to the fiftieth cycle are shown in Fig. 7 at locations A and B for case 1, and locations B and C for case 2. Comparison of these results with the computed creep strain increments from MARC for the first two cycles indicate fair agreement. The one dimensional analysis predicts somewhat higher creep strains for the initial cycle, but exaggerates the amount of stress relaxation with the result that lower creep strain increments were predicted for the second cycle. The slower stress relaxation shown by the three dimensional analysis was probably caused by the greater constraints due to the multi-axial stress-strain state. Fig. 7 indicates that the mission analyses should be carried out to at least the third cycle in order to attain a reasonably stable stress and creep strain state. The calculated maximum total strain ranges from the beam-type analyses were about twice the three dimensional results, primarily due to predicting higher residual strains on unloading.

Considering the relative simplicity and rapid solution time of the one dimensional program, these results indicate that it can be used with fair accuracy for structural analyses of all-impingement cooled airfoil shells when creep is the major damage mechanism. However, this method cannot take into account directly the stress concentration of film cooling holes. Use of a strain concentration factor calculated by the Neuber method resulted in creep strains for the first cycle that were 50 percent lower than the creep strains calculated from the three dimensional analyses of cases 3 and 4.

Life Analyses

Strain cycling fatigue data for IN 100 at 927° C presented in (7) indicate that the fatigue life from repeated cycling over the total strain ranges shown in Table II would be virtually infinite for cases 1 and 2. The fatigue lives for cases 3 and 4 would be at least an order of magnitude greater than the predicted creep lives as determined from a ductility exhaustion approach (8) where the lives were estimated from the number of cycles that would be required for the creep strain increment during the second cycle to exhaust the creep rupture ductility. Therefore, creep is probably the dominant damage mode for all the cases studied.

Crack initiation life predictions are presented in Table II on a nondimensionalized basis with respect to case 1. The predicted life for any case is taken simply as the reciprocal of the ratio of the creep strain increment for that case to the creep strain increment for case 1. The justifications for extending results computed for two cycles over the engine lifetime are twofold. First, the nondimensionalized lives based on the initial cycle were within 6 percent of those based on the second cycle for cases 1, 2, and 3 (this was not true of case 4 because of the change in critical location); and second, the one dimensional analyses for cases 1 and 2 showed that the nondimensionalized creep life of case 2 based on the fiftieth cycle was only 15 percent greater than the life based on the second cycle. The effect of using a flatter gas temperature profile in case 2 was to increase the cyclic creep life of the all-impingement cooled airfoil about 21 percent. The introduction of leading-edge film cooling holes with the holes oriented normal to the airfoil surface resulted in a reduction of 50 percent in cyclic creep life; however, this does not take into account the reduced susceptibility to hot corrosion damage due to the reduced leading edge temperatures. Angling the film cooling holes 30° radially to the surface resulting in a 28 percent reduction in cyclic life compared to the base all-impingement cooling configuration.

SUMMARY OF RESULTS

The results of the mission analyses of impingement cooled airfoils with and without leading-edge film cooling can be summarized as follows:

1. Creep was the predominant damage mode and the leading-edge inside wall was the predicted distress location for all of the airfoil configurations analyzed. Plastic strains were incurred only during the takeoff transient on the initial mission cycle. Predicted fatigue lives based on the maximum total strain ranges were at least an order of magnitude greater than the predicted creep lives as determined from a ductility exhaustion approach.

2. The use of a flatter gas temperature profile, which reduced the maximum gas temperatures at the rotor inlet by 22° C, resulted in a predicted 21 percent improvement in creep life for the all-impingement cooled airfoils.

3. The introduction of leading-edge film cooling holes was detrimental to the creep life although it lowered the leading-edge temperatures (thus reducing the susceptibility to hot corrosion damage). For the same metal temperatures, a hole with the axis angled radially was less detrimental than a hole with the axis normal to the surface.

4. One dimensional structural analyses gave fair agreement with the three dimensional analyses for the all-impingement cooled case; however, they did not give satisfactory results when used, in conjunction with a Neuber strain concentration factor, for the film cooling cases. The best agreement between the two analytical methods was in initially calculating the maximum creep strains and in predicting the airfoil distress location in the leading-edge region, although not in the same location within that region. The one dimensional analyses appear to exaggerate the creep strain relaxation for subsequent cycles and the residual total strains.

REFERENCES

1 "MARC-CDC General Purpose Finite Element Analysis Program." Vol. 1, User Information Manual, Control Data Corp., 1977.

2 "MARC-CDC Program Input," Vol. 2, User Information Manual, Control Data Corp., 1977.

3 Gaugler, R. E.: "TACT1, A Computer Program for the Transient Thermal Analysis of a Cooled Turbine Blade or Vane Equipped with a Coolant Insert." I - User's Manual. NASA TP-1271, 1978.

4 Fritz, L. J.; and Koster, W. P.: "Tensile and Creep Rupture Properties of (16) Uncoated and (2) Coated Engineering Alloys at Elevated Temperatures," NAS CR-135138, 1977.
5 Kaufman, A.: "Steady-State Stress Relaxation Analysis of Turbine Blade Cooling Designs." NASA TN D-5282, 1969.
6 Peterson, R. E.: "Stress Concentration Design Factors." John Wiley and Sons, Inc., 1974.
7 Stewart, O. L.; and Vogel, W. H.: "Methods for Predicting Thermal Stress Cracking in Turbine Stator or Rotor Blades." Rep. PWA-3142, Pratt and Whitney Aircraft (NASA CR-54636), July 10, 1967.
8 Spera, D. A.: "Comparison of Experimental and Theoretical Thermal Fatigue Lives for Five Nickel-Base Alloys." STP-520, Philadelphia, PA. Am. Soc. Testing Mater., 1972.

TABLE I. - ANALYTICAL CASES

Case number	Airfoil cooling configurations	Gas temperature profile
1	All impingement	A
2	All impingement	B
3	Leading-edge film-cooling holes normal to surface, remainder of airfoil impingement cooled	A
4	Leading-edge film-cooling holes 30° to surface, remainder of airfoil impingement cooled	A

Gas temperature, °C

	Profile A	Profile B
Idle	546-680	555-669
Max. takeoff	1169-1400	1187-1378
Max. climb	1119-1342	1136-1321
Cruise	1085-1304	1102-1284

TABLE II. - RESULTS OF MISSION STRAIN ANALYSES

Case	Maximum effective total strain range, idle to max. takeoff, cm/cm	Maximum effective total strain range, max. takeoff to shutdown,[a] cm/cm	Maximum effective creep strain increment, 2nd cycle, cm/cm	Predicted nondimensional cyclic lives[b]
1	[c]0.00141 (.00277)	0.00234	0.000484 (.000427)	1.00
2	0.00162 (.00290)	0.00248	0.000399 (.000351)	1.21
3	0.00468	0.00602	0.000970	0.50
4	0.00453	0.00523	0.000671	0.72

[a]Estimate based on maximum effective total strain during 1st cycle between max. takeoff and idle.
[b]Based on maximum effective creep strain change during 2nd cycle.
[c]Numbers in parentheses refer to results from one dimensional beam-type analyses.

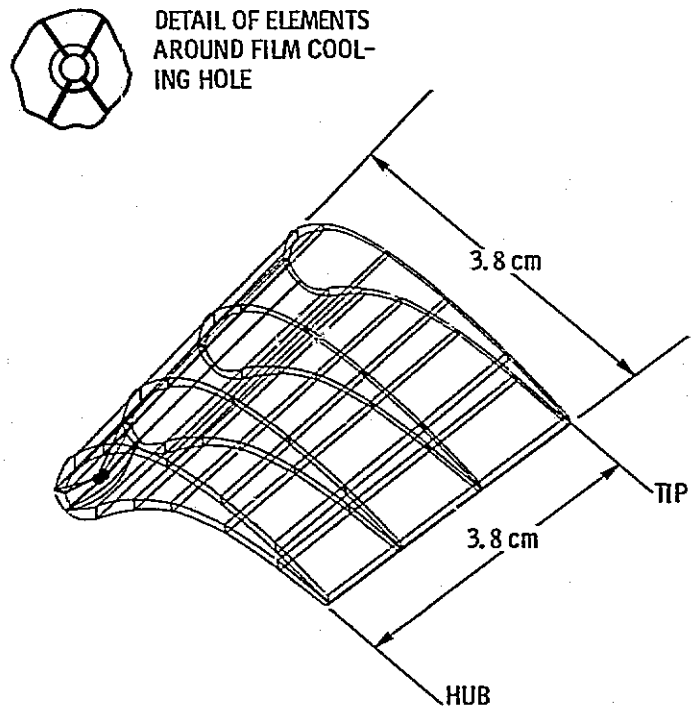

Figure 1. - Airfoil finite element model (leading-edge film cooled blade).

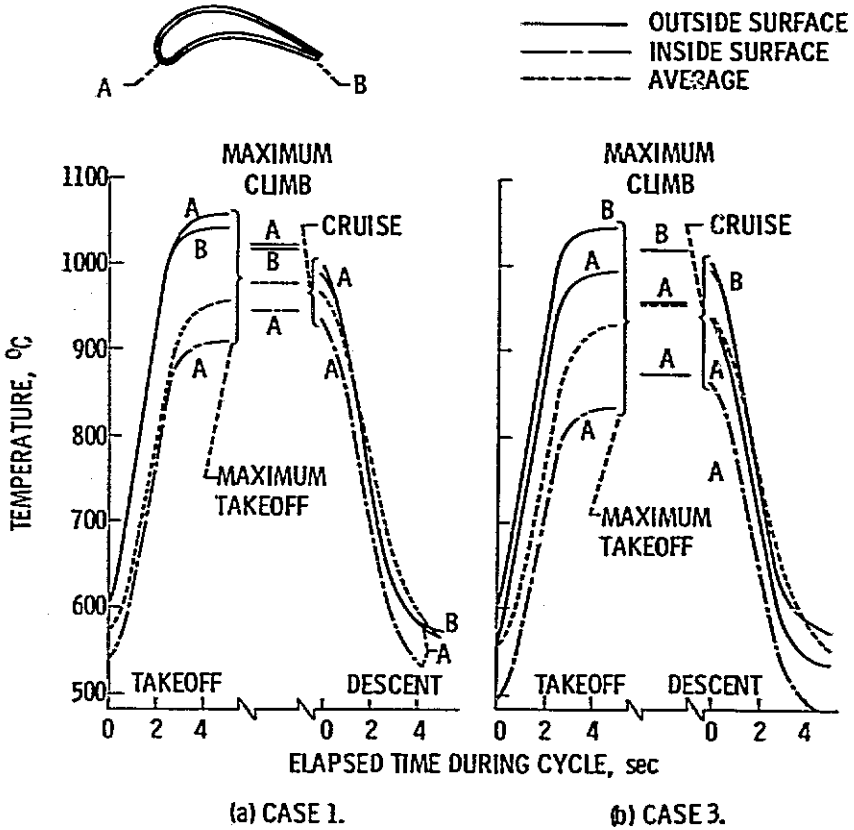

Figure 2. - Airfoil metal temperature cycle at midspan.

	TEMP., °C		TEMP., °C
1	832	6	927
2	849	7	943
3	866	8	966
4	887	9	982
5	904	10	999

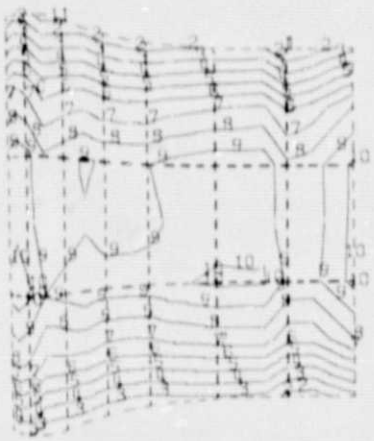

(a) OUTSIDE SURFACE, PRESSURE SIDE.

	TEMP., °C		TEMP., °C
1	827	6	921
2	843	7	943
3	866	8	966
4	882	9	982
5	904	10	1004

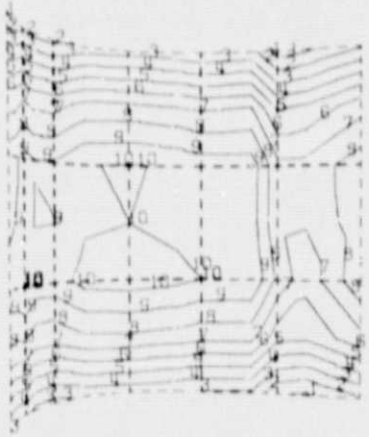

(b) OUTSIDE SURFACE, SUCTION SIDE.

Figure 3. - Airfoil metal temperature distribution at cruise for case 1.

	STRESS, MPa		STRESS, MPa
1	67	6	223
2	98	7	255
3	130	8	286
4	161	9	318
5	192	10	349

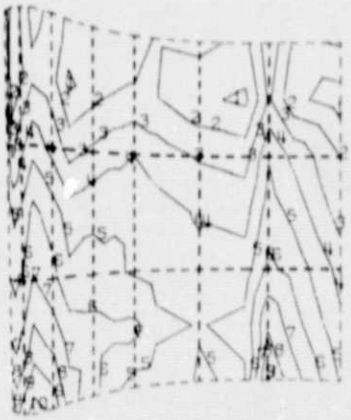

(a) EFFECTIVE STRESS, INSIDE SURFACE, PRESSURE SIDE.

	STRAIN, cm/cm		STRAIN, cm/cm
1	-0.292E-4	6	.699E-3
2	.116E-3	7	.845E-3
3	.262E-3	8	.990E-3
4	.408E-3	9	.114E-2
5	.553E-3	10	.128E-2

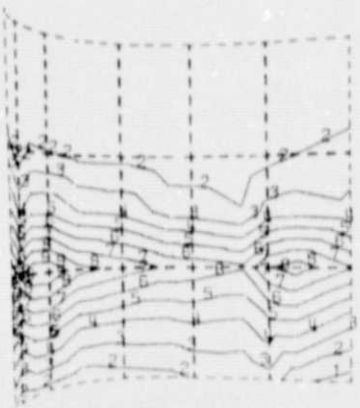

(b) EFFECTIVE CREEP STRAIN, INSIDE SURFACE, SUCTION SIDE.

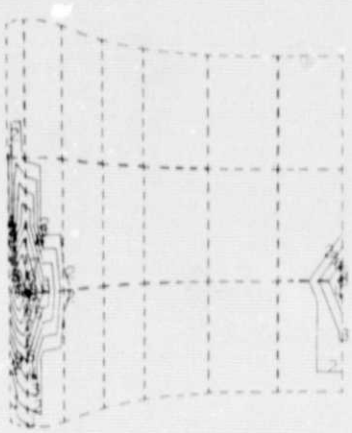

	STRAIN, cm/cm
1	-0.585E-5
2	.106E-4
3	.271E-4
4	.436E-4
5	.601E-4
6	.766E-4
7	.931E-4
8	.110E-3
9	.126E-3
10	.142E-3

(c) EFFECTIVE PLASTIC STRAIN, OUTSIDE SURFACE, PRESSURE SIDE.

Figure 4. - Stress-strain contours at end of cruise, 2nd cycle for case 1.

E-9720

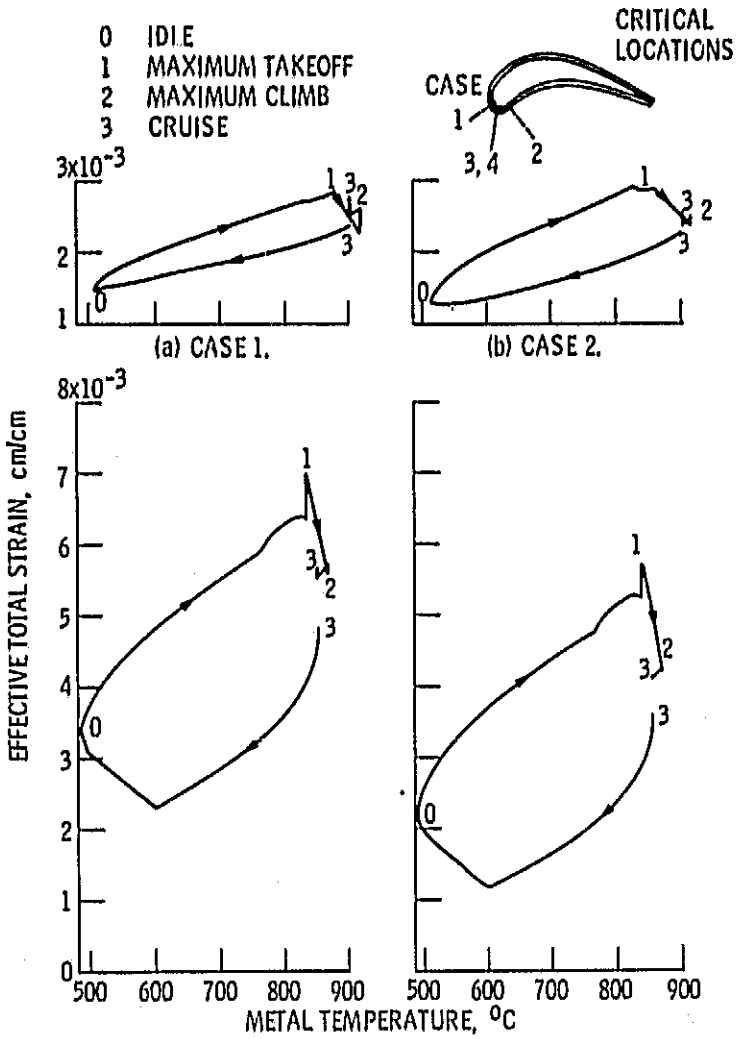

Figure 5. - Effective total strain-temperature cycles for critical airfoil locations.

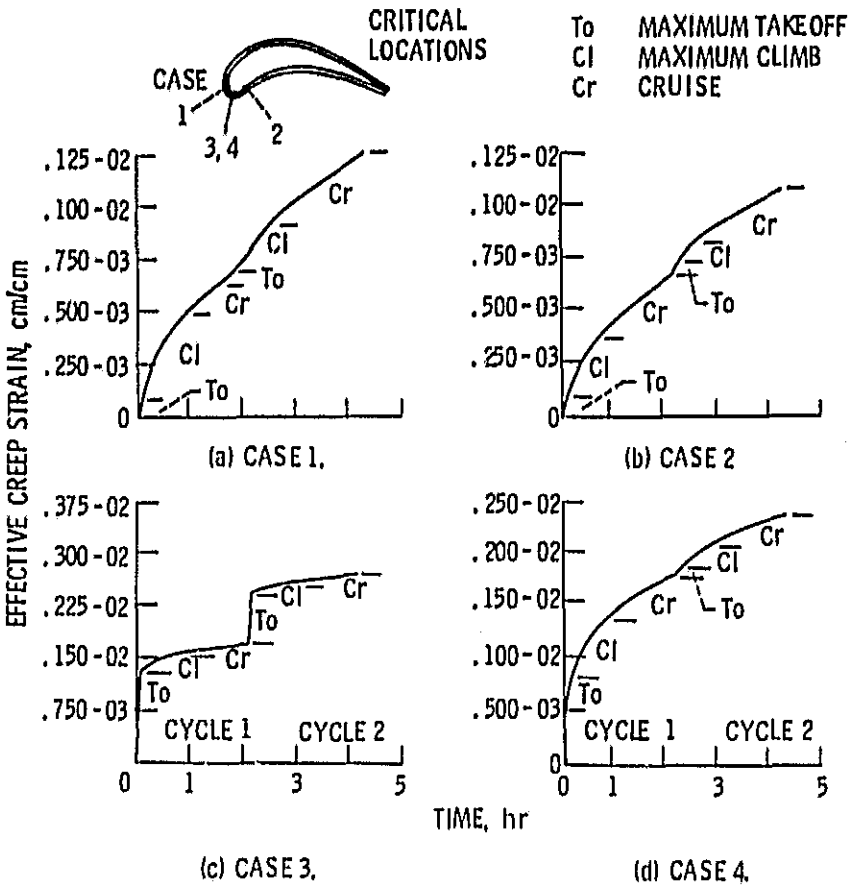

Figure 6. - Effective creep strain as a function of time for critical airfoil locations.

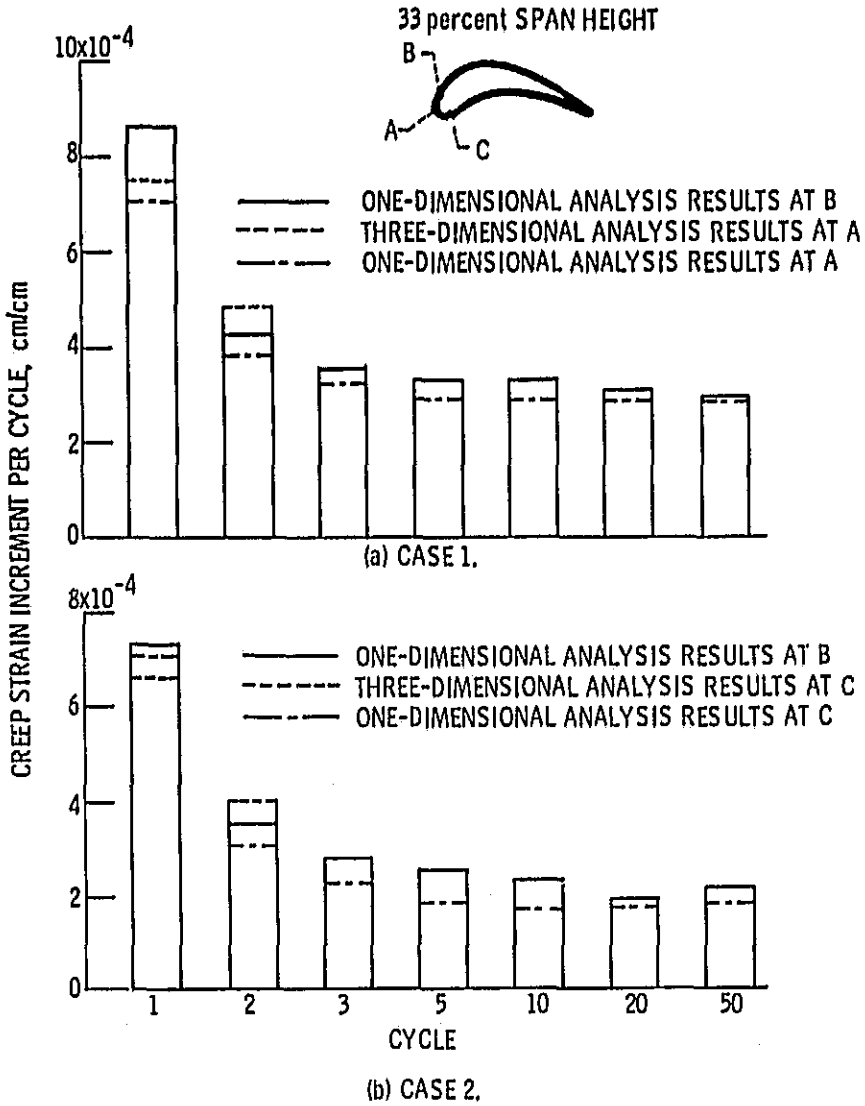

Figure 7. - Comparison of creep strain computations from one- and three-dimensional structural analyses.